### Title
A bio-facilitated synthetic route for nano-structured complex electrode materials




### Journal
Green Chemistry, 18(9)

### ISSN
1463-9262



### Authors
Moradi, Maryam
Kim, Jae Chul
Qi, Jifa
et al.



### Publication Date
2016

### DOI
10.1039/c6gc00273k

Peer reviewed

Green Chemistry

COMMUNICATION

View Article Online
View Journal

Cite this: DOI: 10.1039/c6gc00273k

Received 28th January 2016,
Accepted 18th February 2016

DOI: 10.1039/c6gc00273k

www.rsc.org/greenchem

# A bio-facilitated synthetic route for nano-structured complex electrode materials†

Maryam Moradi,[a,b,c] Jae Chul Kim,‡[a,d] Jifa Qi,‡[a,b,c] Kang Xu,[e] Xin Li,[a] Gerbrand Ceder[a,d,f] and Angela M. Belcher*[a,b,c]

**We investigate an energy-efficient synthesis that merges the bio-templated technique and solid-state reactions to produce nano-structured lithiated polyanions. With the aid of bio-templates based on an M13 virus, the thermal budget of an annealing process can be reduced, and the nano-structured characteristics of the precursors are preserved in the product. This method enables us to successfully prepare monoclinic $LiMnBO_3$ with an average particle size of 20 nm in a 1 h annealing process, showing improved electrochemical properties compared with the conventionally synthesized one. Thus, we consider that this bio-facilitated method can open up an environmentally-friendly pathway to produce nano-structured electrode materials with an enhanced performance.**

A solid-state reaction that involves ball-milling and high-temperature firing processes has been often considered as an appropriate method to produce inorganic materials for many applications.[1–5] One of the challenges of using conventional solid-state chemistry is to control particle morphologies, especially to generate uniform nano-structures.[5] Synthesis employing bio-templates based on an M13 virus is now a well-established concept to produce nano-sized inorganic materials, such as semiconductors and metal oxides, in a benign solution-based environment.[6–9] The M13 virus shown in Fig. 1a has a wire-shape morphology with an aspect ratio of ~135 consisting of ~2700 major coat proteins (p8) helically wrapped around its DNA.[10,11] Four minor coat proteins, p3, p6, p7, and p9 are located at the two ends of the virus.[10,11] The functionality of each coat protein can be modified by altering the M13 genome, so that it can bind to the desired material.[12,13]

The functionalized M13 virus on p8 is considered suitable for mineralization of nano-structured metal oxides such as $Co_3O_4$ and $FePO_4$,[13–15] which can be used as electrode materials for rechargeable batteries. The energy storing properties of these electrodes show remarkable improvement in comparison with their conventionally fabricated versions.[13,14] However, producing some materials such as lithiated polyanionic compounds as a cathode for Li-ion batteries is still a nontrivial task due to the nature of the solution-based synthesis.[14] To extend the bio-templated method to produce advanced electrode materials, we have designed a low thermal-budget synthesis that merges the M13 virus-templated solution-based technique with solid-state chemistry.

In this work, we apply this technique to synthesize a Li storage nanomaterial, monoclinic lithium manganese borate ($LiMnBO_3$), which has been obtained mostly by conventional methods to date.[16–18] This borate composition shows polymorphism in hexagonal and monoclinic structures and has a high theoretical capacity of 220 mA h $g^{-1}$ with good phase stability.[18,19] However, both polymorphs show limited capacities in battery tests, likely originating from sluggish Li mobility due to the nature of one-dimensional diffusion.[20] The key to address this issue is to minimize the particle size along with applying a conductive coating[20] and/or substituting a portion of Mn with Fe.[21,22] In hexagonal $LiMnBO_3$, nanosizing indeed improves the achievable capacity in combination with carbon coating as it reduces the solid-state $Li^+$ diffusion length and leads to better electrical wiring in the cathode.[23,24] Unlike the hexagonal polymorph, it is difficult to produce uniform nano-structured monoclinic $LiMnBO_3$ by a conventional solid-state method: low temperature firing often leads to the

[a]Department of Materials Science and Engineering, Massachusetts Institute of Technology, Cambridge, MA 02139, USA. E-mail: belcher@mit.edu
[b]David H. Koch Institute for Integrative Cancer Research, Massachusetts Institute of Technology, Cambridge, MA 02139, USA
[c]Department of Biological Engineering, Massachusetts Institute of Technology, Cambridge, MA 02139, USA
[d]Materials Science Division, Lawrence Berkeley National Laboratory, Berkeley, California 94720, USA
[e]Power and Energy Division Sensor and Electron Devices Directorate, U.S. Army Research Laboratory, Adelphi, Maryland 20783, USA
[f]Department of Materials Science and Engineering, University of California, Berkeley, California 94720, USA

†Electronic supplementary information (ESI) available: Raman spectroscopy of the virus:SWCNT complex, first cycle behaviour of the bio-templated $LiMnBO_3$, bio-templated $LiMnBO_3$ : SWCNT, and conventionally prepared $LiMnBO_3$. See DOI: 10.1039/c6gc00273k

‡These authors contributed equally.

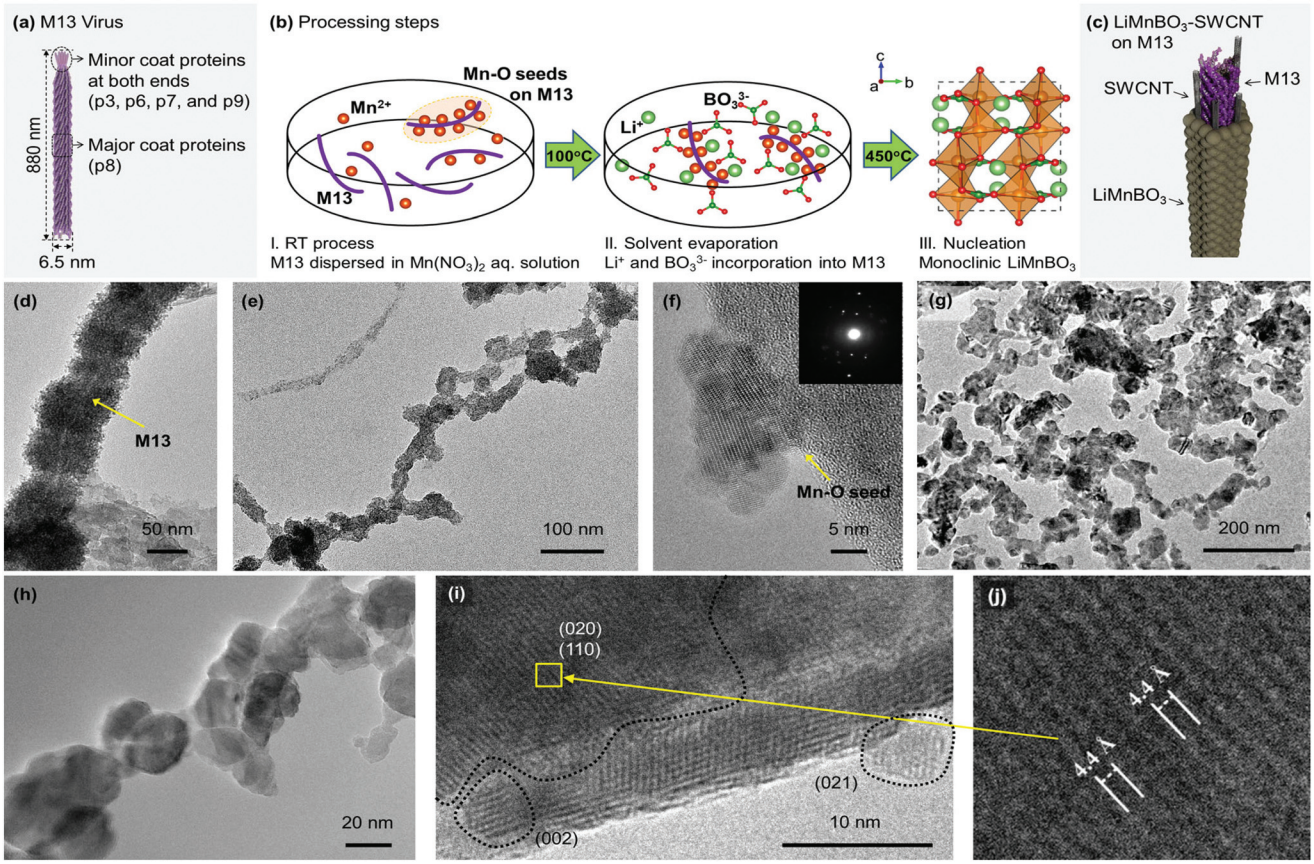


**Fig. 1** (a–j). Schematic representations of the developed synthetic method showing (a) the M13 virus, (b) processing steps for $LiMnBO_3$ production, and (c) $LiMnBO_3$ on the M13-SWCNT complex. (d–j). (HR)TEM images of the bio-templated (d and e) nanowire-shaped seed structure in different magnifications, (f) precipitated manganese oxides on the M13 virus, (g–j) $LiMnBO_3$ particles after annealing at different magnifications.

incomplete reaction and/or secondary phases, and high temperature firing enlarges the particle size.[18,25] Our method aims to nucleate the precursor materials (Mn, Li, $BO_3$) onto the genetically engineered M13 virus, so that the annealing thermal budget, such as the firing temperature and time, can be reduced to form monoclinic $LiMnBO_3$ while maintaining the nano-structure.

To use $LiMnBO_3$ as a battery cathode, a coating of electronically conductive phases is generally required to form percolated pathways for electron conduction.[18] With the aid of the M13 virus, we also integrate single walled carbon nanotubes (SWCNTs) as the conductive phase into the active material with a high surface contact area to facilitate electron transport throughout the electrode.[14] As we only investigate the monoclinic polymorph of $LiMnBO_3$, it will be hereafter denoted as $LiMnBO_3$ without referring to the structure.

## Bio-templated synthesis

Our synthesis method for $LiMnBO_3$ features three steps, as shown in Fig. 1b: (I) formation of manganese oxides on the M13 virus template as a seed structure, (II) incorporation of lithium and borate ions over the seeds to produce $LiMnBO_3$ precursors, and (III) a 1 h annealing process under a reducing (mixture of 4% $H_2$ + 96% Ar) atmosphere at 450 °C to obtain the final products. The developed procedure can keep the relatively long time of ball-milling and firing processes that are conventionally used for $LiMnBO_3$ synthesis.[16–18]

We optimize the specific M13 virus with the p8 insert sequence of DSPHTELP not only to mineralize the seed material but also to bind SWCNTs onto the material. DSPHTELP has a histidine (H), an aromatic residue that could interact with SWCNTs through π–π stacking at all pH ranges. By using this specific virus, the surface contact between the active inorganic material and SWCNTs can be maximized. The bio-templated material of the M13-SWCNT complex is depicted in Fig. 1c.

To facilitate the development of bio-templated $LiMnBO_3$, the M13 virus is incubated with manganese ions in an aqueous $Mn(NO_3)_2$ solution for 2 h at room temperature (RT). The virus surfaces are negatively charged at a pH above 5.3.[26] During the nucleation, the pH of the solution is kept approximately at 6 (Zeta potential of −20 mV)[26] to ensure its electro-

 

static binding to manganese ions. Manganese oxides are precipitated on the M13 virus immediately after adding lithium hydroxide to the solution. The material is then washed with deionized water and collected through filtration. To form $LiMnBO_3$, a stoichiometric ratio of lithium hydroxide and boric acid is mixed with the bio-templated manganese oxide in an aqueous solution. The solution is heat-treated at 100 °C with stirring to evaporate the solvent. This step leads to the manganese oxide seeds being covered with lithium and borate precursors at the nanometer-scale, so that they can serve as nucleation sites for $LiMnBO_3$. Unlike the traditional solid-state synthesis, our approach requires only a short annealing process to remove the water from the structure and transform the materials into $LiMnBO_3$ products. It should be emphasized that optimizing the annealing conditions is very critical to preserve the seed structures, forming functional particles at the nanoscale.

Fig. 1d–j show images obtained from transmission electron microscopy (TEM, accelerating voltage of 200 keV on JEOL 2010F) throughout the bio-templated synthesis process. Fig. 1d–f represent results obtained from the process step I (Fig. 1b). The M13 virus as a bio-template for seed materials can be clearly seen, as marked by an arrow in Fig. 1d. This complex material has a wire-shaped morphology, as shown in Fig. 1e, resulting from the mineralization process of the M13 virus. The seed particles are well-crystalized, having a size ranging from 10 to 20 nm in Fig. 1f. Fig. 1g–j show the morphology of $LiMnBO_3$ after 1 h annealing at 450 °C as a result of process steps II and III in Fig. 1b. The material still maintains the nano-structure template by using the M13 virus after the heat treatment, and the obtained average particle size is approximately 20 nm.

Fig. 2 shows X-ray diffraction (XRD, Cu-$K_\alpha$ radiation on a PANalytical X-ray diffractometer) patterns of the bio-templated Li–Mn–B–O seed material annealed at different temperatures. All samples were annealed for 1 h under a reducing atmosphere. The broad width of the XRD patterns implies that the particles are nanosized. In Fig. 2a, manganese oxide ($Mn_3O_4$) is observed as the main phase at an annealing temperature of 350 °C. As the temperature increases to 400 °C, monoclinic $LiMnBO_3$ appears while a large amount of $Mn_3O_4$ still remains unreacted. At 450 °C, monoclinic $LiMnBO_3$ becomes the major phase. The estimated crystallite size calculated from full width at half maximum of the peaks is about 30 nm, which agrees with the TEM observation in Fig. 1h. This average particle size of $LiMnBO_3$ is significantly smaller than what can be obtained from the conventional method (~100 nm). The elemental concentration of the specimen was characterized with inductive coupled plasma emission spectroscopy and confirms the stoichiometric ratio of Li, Mn, and B. Thus, crystalline $LiMnBO_3$ is successfully synthesized and nanosized *via* the bio-templated technique. Further increasing the annealing temperature to 500 °C leads to the formation of a hexagonal polymorph, making the specimen a two-phase (monoclinic and hexagonal) $LiMnBO_3$ composite. This is consistent with the previous report that uses the solid-state reaction.[18]

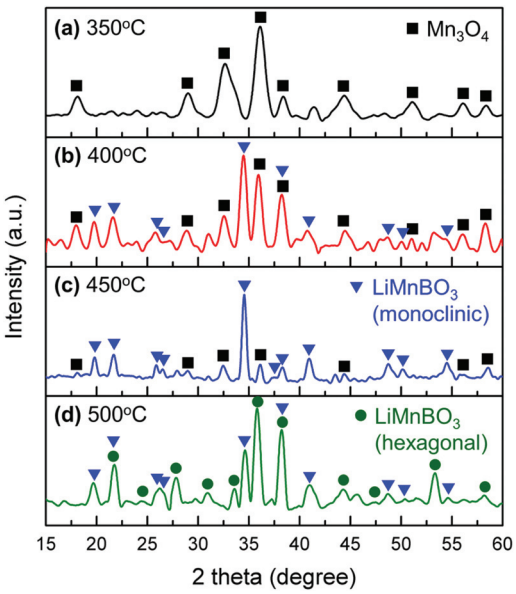


**Fig. 2** XRD patterns of Li–Mn–B–O after annealing at (a) 350 °C, (b) 400 °C, (c) 450 °C, and (d) 500 °C. Phase identification is based on diffraction data in the inorganic crystal structure database: 01-073-4014 for monoclinic $LiMnBO_3$, 01-070-8322 for hexagonal $LiMnBO_3$, and 01-075-1560 for $Mn_3O_4$.

We also integrate SWCNTs into $LiMnBO_3$ by using the same M13 bio-template. SWCNTs were uniformly bound using molecular recognition on the major surface of the virus. Approximately ten SWCNTs were self-assembled along the longitudinal axis of the single M13 virus before mineralization of $LiMnBO_3$ (ref. 26 for detailed procedures).[26] The Raman spectrum of the M13-SWCNT after the complexation process confirms the presence of a SWCNT (ESI, Fig. S1†) in the material. The spectrum peaks match with radial breathing mode peaks and the G peak from SWCNTs.[27] It should be noted that there is no significant difference in the particle morphology and structure of $LiMnBO_3$ before and after attaching SWCNTs according to Fig. S1d–f (ESI†).

### Electrochemical performance of bio-templated $LiMnBO_3$

To study the electrochemical performance of the bio-templated $LiMnBO_3$ and $LiMnBO_3$–SWCNTs as a cathode for Li-ion batteries, films were prepared by mixing $LiMnBO_3$, Super P carbon, and PTFE binder with a mass ratio of 70 : 25 : 5. The large carbon content is to ensure a good electronic contact between the active particles in the cathode. The mixture was rolled and cut with a loading of 4 mg $cm^{-2}$, approximately. Coin cells were assembled in an argon-filled glove box with the cathode film, Li metal as an anode, and 1 M $LiPF_6$ in ethylene carbonate and dimethyl carbonate (3 : 7 by volume) with 5 mM tris(hexafluoro-iso-propyl)phosphate (HFiP) as an electrolyte.[28] The cells were cycled in the galvanostatic mode in a voltage range between 2 and 4.6 V on a Solartron Analytical 1470E potentiostat at RT. A 1C rate corresponds to the current of the

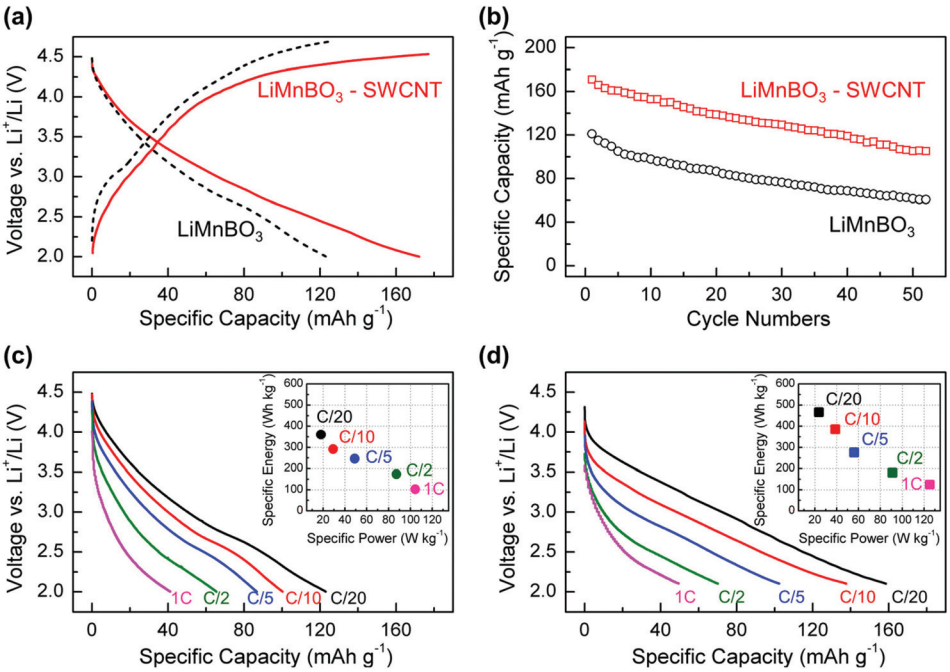


**Fig. 3** Electrochemical performance of the $LiMnBO_3$ and $LiMnBO_3$–SWCNTs: (a) voltage profiles as a function of specific capacity at a C/20 rate, (b) capacity retention, and voltage-capacity and specific energy-specific power at different discharge rates in (c) $LiMnBO_3$ and (d) $LiMnBO_3$–SWCNTs.

fully discharging theoretical capacity of $LiMnBO_3$, 220 mA $g^{-1}$, in 1 h.

Fig. 3a shows the voltage profile of the bio-templated $LiMnBO_3$ and $LiMnBO_3$–SWCNT cathodes in a representative (second) cycle at a C/20 rate. The achieved charge and discharge capacities of $LiMnBO_3$ are 130 and 125 mA h $g^{-1}$, respectively. Although these capacities do not reach the theoretical value (220 mA h $g^{-1}$), they surpass what conventionally synthesized $LiMnBO_3$ consisting of larger particles normally achieves at the same rate without carbon coating, as shown in Fig. S2 (ESI†) and reported in the literature.[18,29] This directly demonstrates how nanosizing of $LiMnBO_3$ improves the battery performance. The $LiMnBO_3$–SWCNT cathode delivers 180 and 173 mA h $g^{-1}$ in charge and discharge respectively, which is a sharp increase compared to the results obtained from bio-templated $LiMnBO_3$ without SWCNTs (~125 mA h $g^{-1}$) in Fig. 3a and conventional carbon coated $LiMnBO_3$ (~100 mA h $g^{-1}$) in Fig. S2.† The capacity retention of $LiMnBO_3$ with and without SWCNTs is plotted in Fig. 3b, indicating the reversibility of the cell capacity at an average fading rate of 1.1% and 1.3% per cycle, respectively.

Fig. 3c and d show the rate capability of the bio-templated $LiMnBO_3$ and $LiMnBO_3$–SWCNT cathodes. Increasing the current density from C/20 to 1C, the discharge capacity of $LiMnBO_3$ decreases from 125 to 42 mA h $g^{-1}$ in Fig. 3c. This rate dependency may originate from incomplete electrical wiring that leads to high impedance in the electrode.[30] For $LiMnBO_3$–SWCNT, the effect of SWCNT incorporation can be clearly observed from the improved rate capability in Fig. 3d. A higher capacity is not only achieved at C/20, but also at various higher rates (50 mA h $g^{-1}$ at 1 C). The specific energy and specific power in $LiMnBO_3$–SWCNTs at discharge are also enhanced in comparison with those in $LiMnBO_3$ without SWCNTs, as shown in the insets of Fig. 3c and d. At C/20, the obtained specific energy for $LiMnBO_3$–SWCNTs is 466 Wh $kg^{-1}$ and 360 Wh $kg^{-1}$ for $LiMnBO_3$. The reported energy for the $LiMnBO_3$ cathode from solid-state methods is much lower than those values, approximately 275 Wh $kg^{-1}$.[22] Therefore, our results on the $LiMnBO_3$–SWCNT cathode show a significant progress in improving the battery properties of $LiMnBO_3$, which is enabled by employing the biological toolkit for nanoparticle synthesis.

The particle size of polyanionic cathode materials plays a significant role in determining the Li intercalation activity,[20,31] and we demonstrate how nano-sized particles promote the overall capacity of $LiMnBO_3$ in Fig. 3. $LiMnBO_3$ synthesized at around 500 °C likely involves a fair amount of atomic disorder between Li and Mn (*i.e.*, antisite disorder) with an average particle size of 100 nm.[19,20] Moreover, *ab initio* studies revealed that Li diffuses along the *c*-axis in the monoclinic as well as the hexagonal $LiMnBO_3$ lattices (one-dimensional diffusion).[18] As a result, the antisite disorder can disrupt Li transport in $LiMnBO_3$ by blocking its diffusion pathway and limit the accessibility to Li inside particles from the surface, especially in the case where the cathode is composed of large particles (>100 nm).[20,31] The implication here is that the path-blocking antisites unlikely influence the activity of Li at the surface. As the synthesis temperatures of conventionally prepared and bio-templated $LiMnBO_3$ do not vary significantly, a similar amount of antisite may exist in both materials with the same

 

crystal structure. Thus, we consider that a bio-templated $LiMnBO_3$–SWCNT effectively circumvents the negative aspect of the antisite disorder on Li intercalation with a proliferating surface-to-volume ratio of the nanosized, 20 nm, particles.

It should be emphasized that nanosizing generally increases the degree of particle agglomeration that often hinders complete electrical contact between the individual particles and the conductive matrix in the electrode.[32] In our study, the self-assembly of the nano-structured active material may reduce the agglomeration as $LiMnBO_3$ particles tend to be aligned along the M13 virus as it provides the nucleation sites. Moreover, we show that by integrating approximately 3 wt% SWCNTs into $LiMnBO_3$, 82% of the theoretical capacity is achieved. The improved electrochemical activity can be directly related to the better cross-linking of electron conducting pathways throughout the electrode[30] as SWCNTs can percolate with each other during the formation of $LiMnBO_3$ particles in an *in situ* fashion. As a result, inter-particle impedance within the electrode significantly reduces, and polarization of the cell decreases, so that a higher capacity can be delivered.

Still, $LiMnBO_3$ and $LiMnBO_3$–SWCNT cathodes need to improve their cyclability to be considered as practical materials. The notable capacity fading of $LiMnBO_3$ can be attributed to the intrinsic instability of its charged state, leading to the loss of the active mass by phase decomposition and/or Mn dissolution, as reported by Kim *et al.*[33] However, given that partial Fe or Mg substitution for Mn can stabilize the charged structure, and surface treatment to form glassy coatings can reduce Mn dissolution,[21,22,33] there is room for improvement of the cyclability of this material.

It should be noted that using a virus template may add an extra step to the synthesis conditions of the routine solid-state method. However, by combining the bio-templated technique with the solid-state chemistries, we can successfully obtain a well-crystallized phase with uniformly nanosized $LiMnBO_3$ particles, which has not been achievable from conventional ceramic processing. We believe that this work can be a good demonstration of how to produce similar inorganic materials that need nanosizing and crystallization.

## Conclusions

We have demonstrated a low thermal budget synthesis method to produce nano-structured inorganic compounds for Li-ion batteries. By employing the M13 virus as a template, the solution-based and solid-state methods can be combined, forming the target material with a shorter processing time and lower thermal budget as compared to conventional solid-state procedures. The M13 virus helps to arrange the nanometer size precursors at a close distance to each other so that only a short annealing process is required to form the final product. As a result, no downsizing techniques such as ball-milling or attrition are required, which is necessary to promote Li diffusion in order for the battery material to achieve a large energy storing performance.

## Acknowledgements

This study was supported by the Institute for Collaborative Biotechnologies through grant W911NF-09-0001 from the U.S. Army Research Office. The content of the information does not necessarily reflect the position or the policy of the Government, and no official endorsement should be inferred. J. C. Kim, X. Li, and G. Ceder acknowledge Robert Bosch GmbH, Umicore, and the MRSEC Program of the National Science Foundation under award number DMR-0819762 and by the Assistant Secretary for Energy Efficiency and Renewable Energy, Office of Vehicle Technologies of the U.S. Department of Energy under Contract no. DE-AC02-05CH11231, under the Batteries for Advanced Transportation Technologies (BATT) Program for financial support.

## Notes and references

1 R. L. Coble and W. D. Kingery, *J. Am. Ceram. Soc.*, 1956, **39**, 377–385.
2 S. M. Haile, *Acta Mater.*, 2003, **51**, 5981–6000.
3 Y. Saito, H. Takao, T. Tani, T. Nonoyama, K. Takatori, T. Homma, T. Nagaya and M. Nakamura, *Nature*, 2004, **432**, 84–87.
4 M. E. Song, J. S. Kim, M. R. Joung, S. Nahm, Y. S. Kim, J. H. Paik and B. H. Choi, *J. Am. Ceram. Soc.*, 2008, **91**, 2747–2750.
5 J. M. Tarascon and M. Armand, *Nature*, 2001, **414**, 359–367.
6 S. W. Lee, S. K. Lee and A. M. Belcher, *Adv. Mater.*, 2003, **15**, 689–692.
7 S. W. Lee, C. B. Mao, C. E. Flynn and A. M. Belcher, *Science*, 2002, **296**, 892–895.
8 P. Y. Chen, R. Ladewski, R. Miller, X. N. Dang, J. F. Qi, F. Liau, A. M. Belcher and P. T. Hammond, *J. Mater. Chem. A*, 2013, **1**, 2217–2224.
9 C. Rosant, B. Avalle, D. Larcher, L. Dupont, A. Friboulet and J. M. Tarascon, *Energy Environ. Sci.*, 2012, **5**, 9936–9943.
10 D. A. Marvin, *Curr. Opin. Struct. Biol.*, 1998, **8**, 150–158.
11 D. A. Marvin, L. C. Welsh, M. F. Symmons, W. R. P. Scott and S. K. Straus, *J. Mol. Biol.*, 2006, **355**, 294–309.
12 D. Y. Oh, X. N. Dang, H. J. Yi, M. A. Allen, K. Xu, Y. J. Lee and A. M. Belcher, *Small*, 2012, **8**, 1006–1011.
13 K. T. Nam, D. W. Kim, P. J. Yoo, C. Y. Chiang, N. Meethong, P. T. Hammond, Y. M. Chiang and A. M. Belcher, *Science*, 2006, **312**, 885–888.
14 Y. J. Lee, H. Yi, W. J. Kim, K. Kang, D. S. Yun, M. S. Strano, G. Ceder and A. M. Belcher, *Science*, 2009, **324**, 1051–1055.
15 M. Moradi, Z. Li, J. F. Qi, W. T. Xing, K. Xiang, Y. M. Chiang and A. M. Belcher, *Nano Lett.*, 2015, **15**, 2917–2921.
16 V. Legagneur, Y. An, A. Mosbah, R. Portal, A. L. La Salle, A. Verbaere, D. Guyomard and Y. Piffard, *Solid State Ionics*, 2001, **139**, 37–46.

17 P. Barpanda, D. Dwibedi, S. Ghosh, Y. Kee and S. Okada, *Ionics*, 2015, **21**, 1801–1812.
18 J. C. Kim, C. J. Moore, B. Kang, G. Hautier, A. Jain and G. Ceder, *J. Electrochem. Soc.*, 2011, **158**, A309–A315.
19 D. H. Seo, Y. U. Park, S. W. Kim, I. Park, R. A. Shakoor and K. Kang, *Phys. Rev. B: Condens. Matter*, 2011, 83.
20 J. C. Kim, D.-H. Seo and G. Ceder, *Adv. Energy Mater.*, 2015, **5**, 1401916.
21 A. Yamada, N. Iwane, S. Nishimura, Y. Koyama and I. Tanaka, *J. Mater. Chem.*, 2011, **21**, 10690–10696.
22 J. C. Kim, D. H. Seo and G. Ceder, *Energy Environ. Sci.*, 2015, **8**, 1790–1798.
23 S. Afyon, D. Kundu, F. Krumeich and R. Nesper, *J. Power Sources*, 2013, **224**, 145–151.
24 S. Afyon, D. Kundu, A. J. Darbandi, H. Hahn, F. Krumeich and R. Nesper, *J. Mater. Chem. A*, 2014, **2**, 18946–18951.
25 S. L. Li, L. Q. Xu, G. D. Li, M. Wang and Y. J. Zhai, *J. Power Sources*, 2013, **236**, 54–60.
26 X. N. Dang, H. J. Yi, M. H. Ham, J. F. Qi, D. S. Yun, R. Ladewski, M. S. Strano, P. T. Hammond and A. M. Belcher, *Nat. Nanotechnol.*, 2011, **6**, 377–384.
27 M. S. Dresselhaus, G. Dresselhaus, R. Saito and A. Jorio, *Phys. Rep.*, 2005, **409**, 47–99.
28 A. von Cresce and K. Xu, *J. Electrochem. Soc.*, 2011, **158**, A337–A342.
29 K. J. Lee, L. S. Kang, S. Uhm, J. S. Yoon, D. W. Kim and H. S. Hong, *Curr. Appl. Phys.*, 2013, **13**, 1440–1443.
30 M. Gaberscek, M. Kuzma and J. Jamnik, *Phys. Chem. Chem. Phys.*, 2007, **9**, 1815–1820.
31 R. Malik, D. Burch, M. Bazant and G. Ceder, *Nano Lett.*, 2010, **10**, 4123–4127.
32 P. A. Johns, M. R. Roberts, Y. Wakizaka, J. H. Sanders and J. R. Owen, *Electrochem. Commun.*, 2009, **11**, 2089–2092.
33 J. C. Kim, X. Li, C. J. Moore, S. H. Bo, P. G. Khalifah, C. P. Grey and G. Ceder, *Chem. Mater.*, 2014, **26**, 4200–4206.

 